**Supplementary Information**

# A Crystalline Molecular Gyrotop with Biphenylene Dirotor and its Temperature Dependent Birefringence Change

Atsushi Fujiwara,[a] Yusuke Inagaki,[a] Hiroyuki Momma,[c] Eunsang Kwon,[c] Kentaro Yamaguchi,[b] Manabu Kanno,[d] Hirohiko Kono,[d] and Wataru Setaka*[,a,e]

[a] *Division of Applied Chemistry, Faculty of Urban Environmental Sciences, Tokyo Metropolitan University, 1-1 Minami-Osawa, Hachioji, Tokyo 192-0397, Japan*

[b] *Faculty of Pharmaceutical Sciences at Kagawa Campus, Tokushima Bunri University, 1314-1 Shido, Sanuki, Kagawa 769-2193, Japan*

[c] *Research and Analytical Center for Giant Molecules, Graduate School of Science, Tohoku University, Aoba-ku, Sendai, 980-8578, Japan*

[d] *Department of Chemistry, Graduate School of Science, Tohoku University, Aoba-ku, Sendai, 980-8578, Japan*

[e] *Research Center for Hydrogen Energy-Based Society (ReHES), Tokyo Metropolitan University, Hachioji, Tokyo 192-0397, Japan*

E-mail: wsetaka@tmu.ac.jp

(Total 17 pages including this cover page)

## 1. Copies of NMR and HRMS Spectra for All New Compounds

**a. Spectra of 4,4'-Bis(tri-9-decenylsilyl)biphenyl (2)**

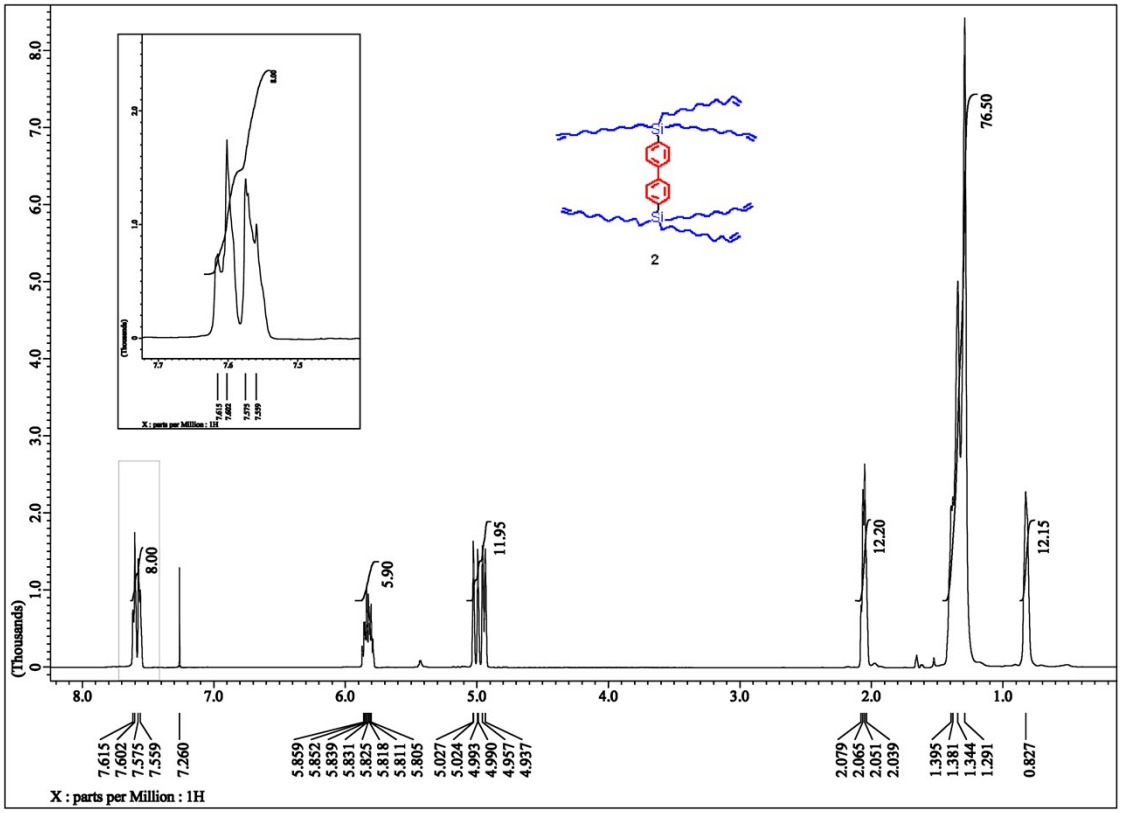


**Fig S1.** $^{1}$H NMR spectrum of 4,4'-Bis(tri-9-decenylsilyl)biphenyl (**2**) in $CDCl_3$.

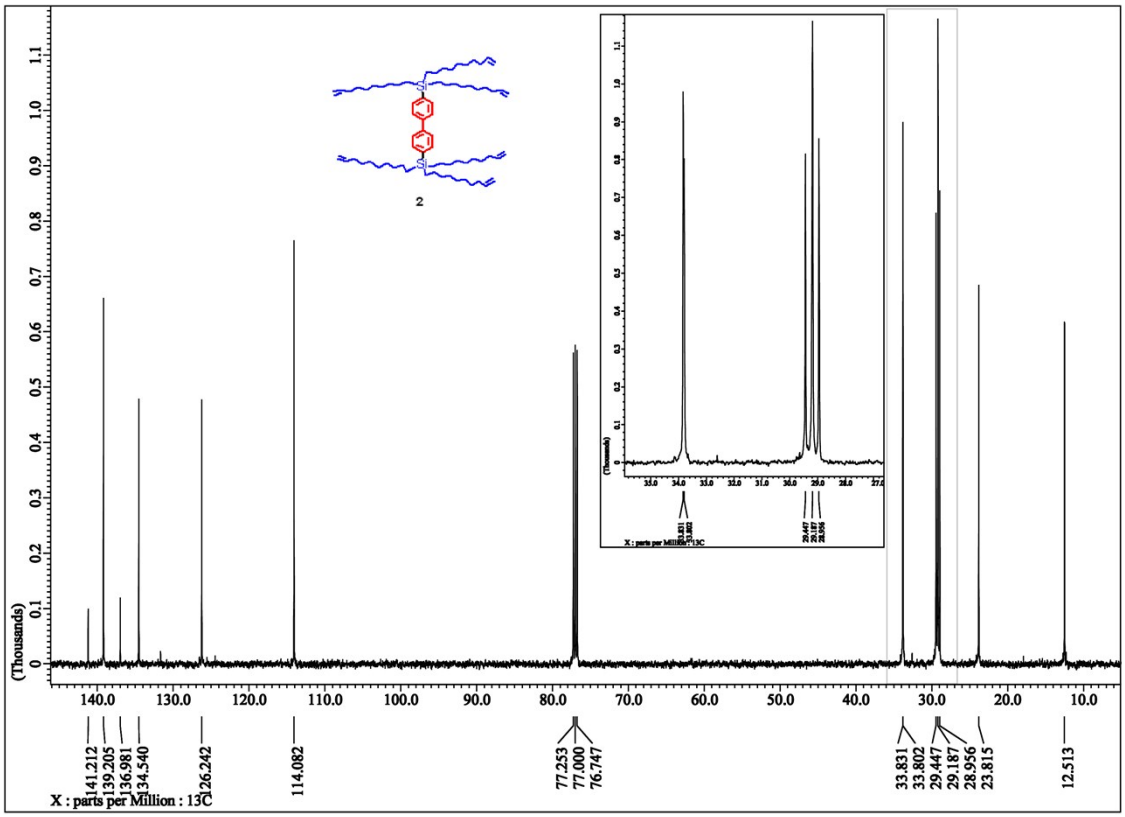


**Fig S2.** $^{13}$C{$^{1}$H} NMR spectrum of 4,4'-Bis(tri-9-decenylsilyl)biphenyl (**2**) in $CDCl_3$.

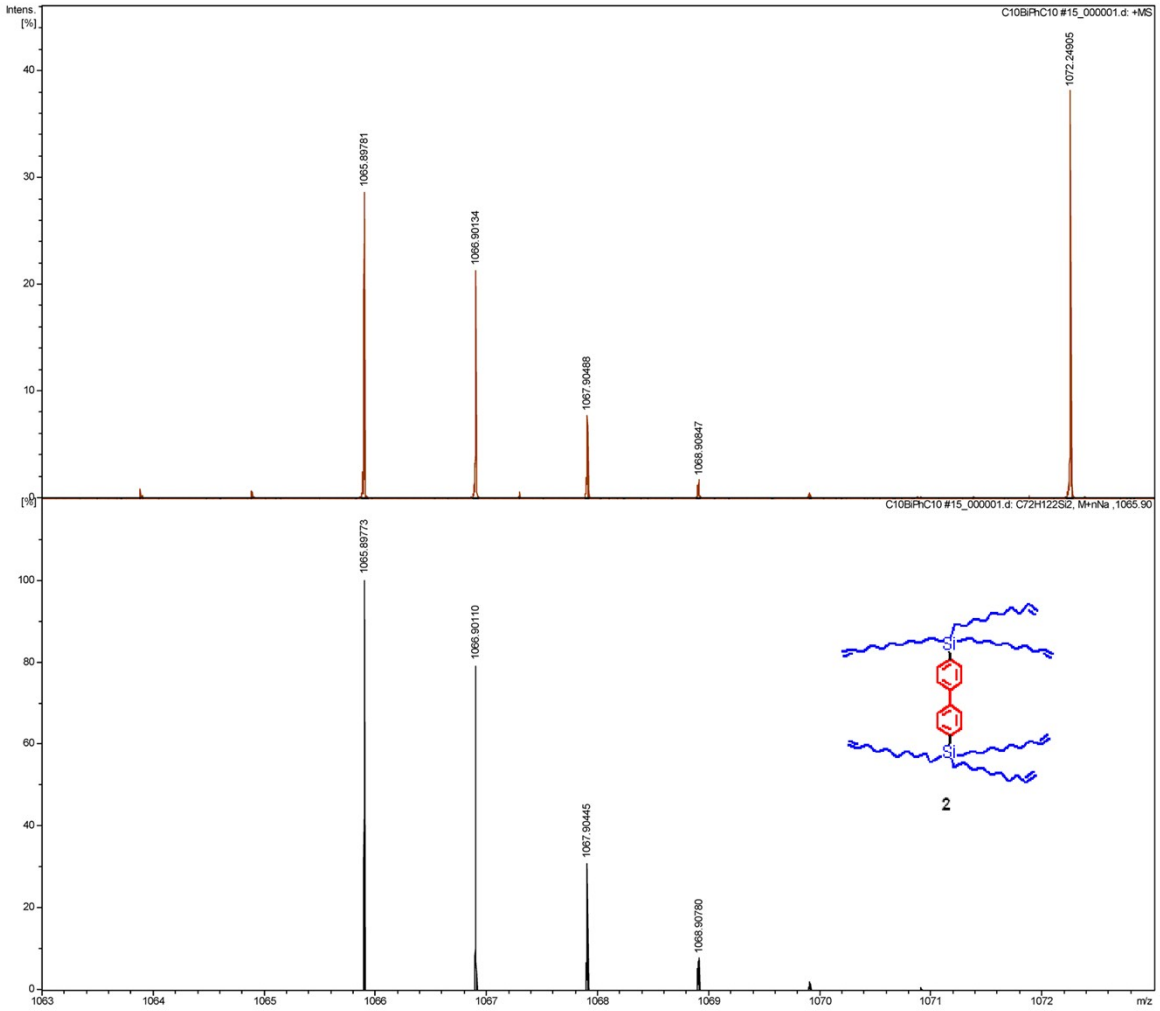


**Fig S3.** HRMS spectrum of 4,4'-Bis(tri-9-decenylsilyl)biphenyl (**2**) (ESI, positive). Top: obsd. Bottom: sim.

**b. Spectra of Biphenylene-bridged Molecular Gyrotop (1)**

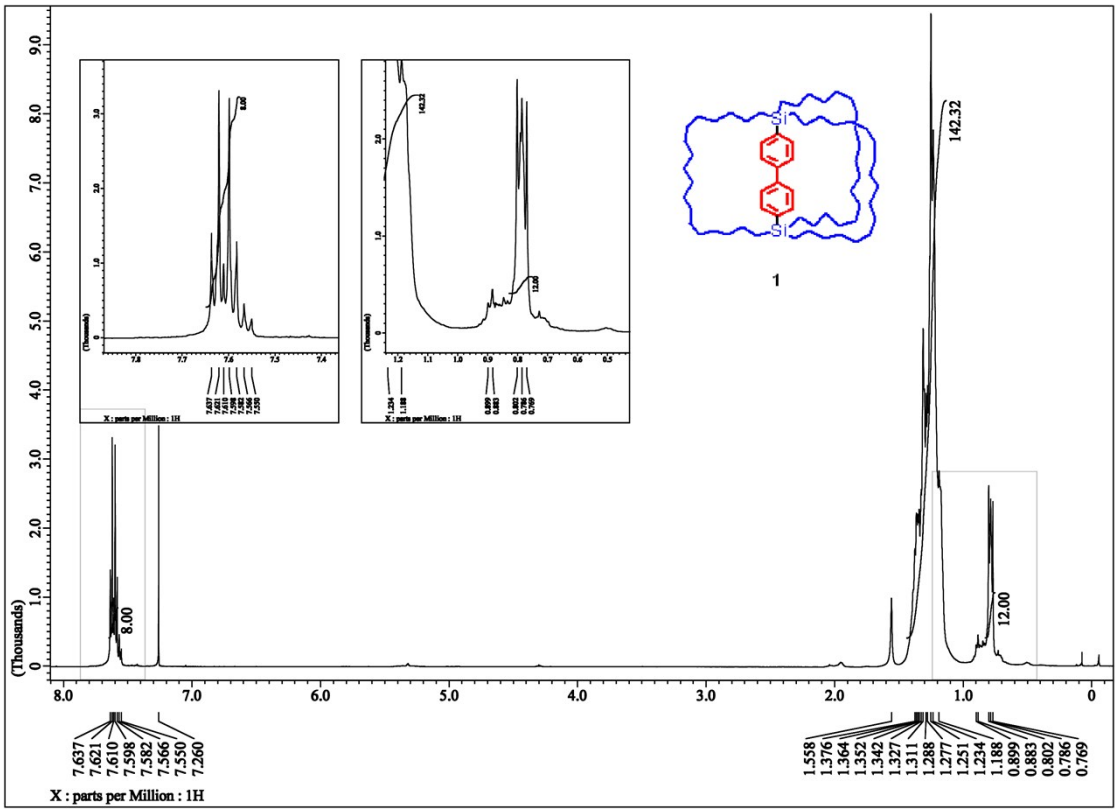


**Fig S4.** $^{1}$H NMR spectrum of Biphenylene-bridged Molecular Gyrotop (**1**) in $CDCl_3$.

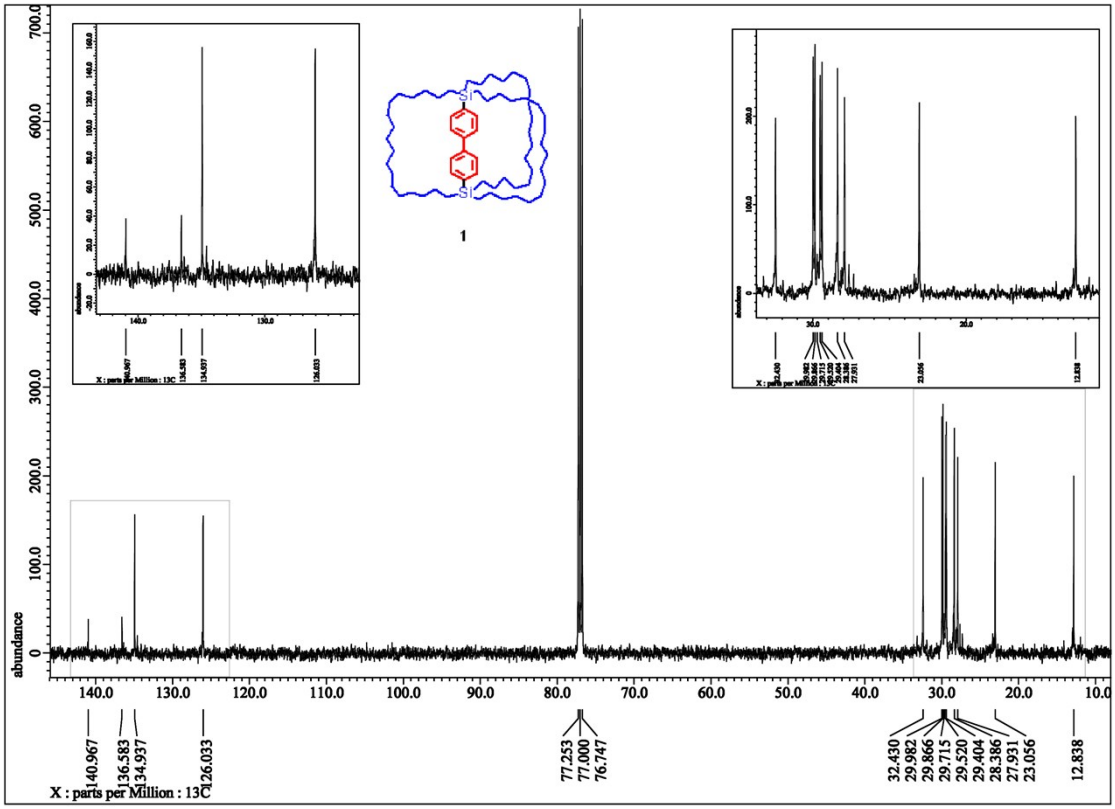


**Fig S5.** $^{13}$C{$^{1}$H} NMR spectrum of Biphenylene-bridged Molecular Gyrotop (**1**) in $CDCl_3$.

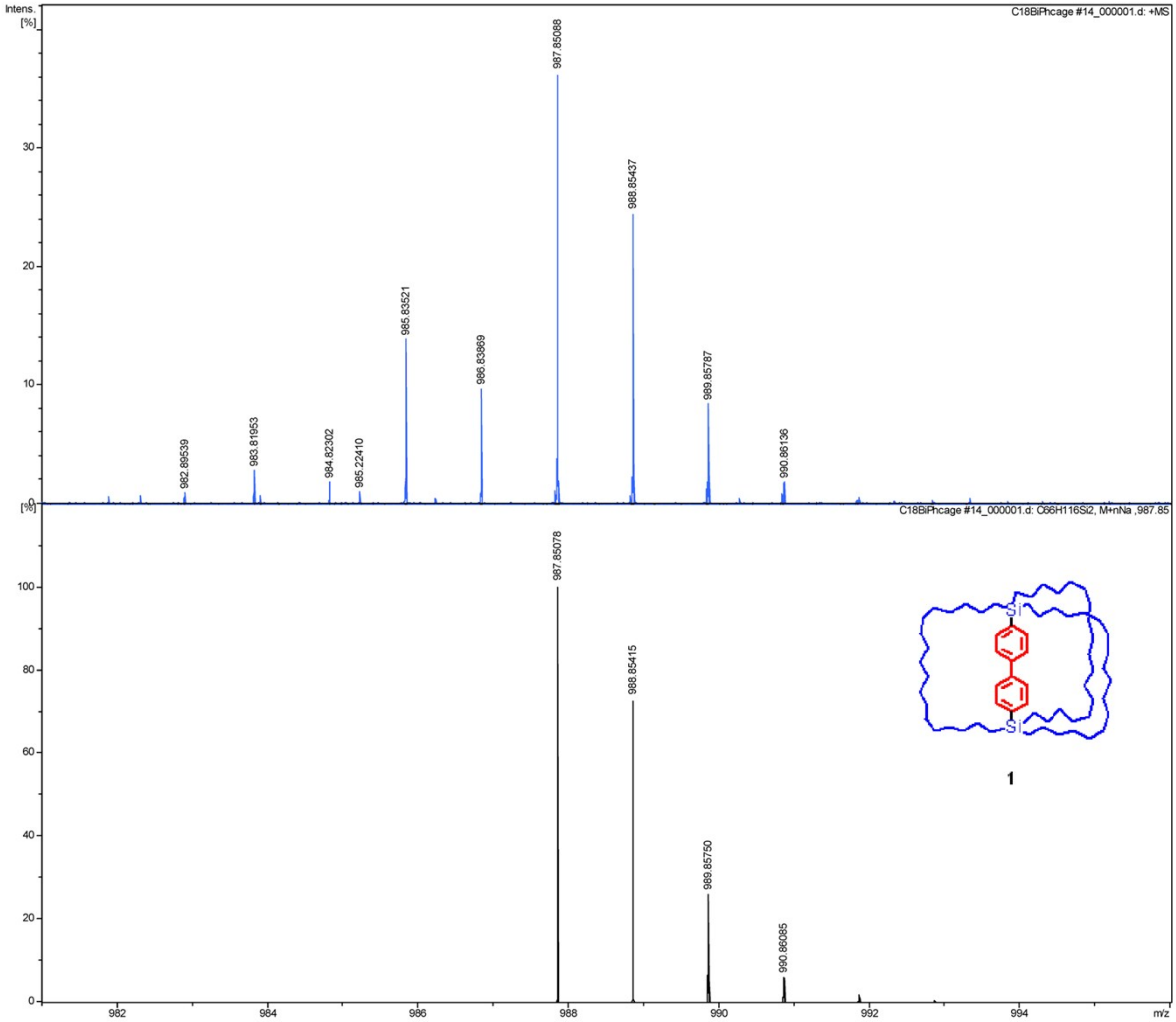


**Fig S6.** HRMS spectrum of Biphenylene-bridged Molecular Gyrotop (**1**) (ESI, positive). Top: obsd. Bottom: sim.

**c. Spectra of Biphenylene-bridged Molecular Gyrotop Isomer (1i)**

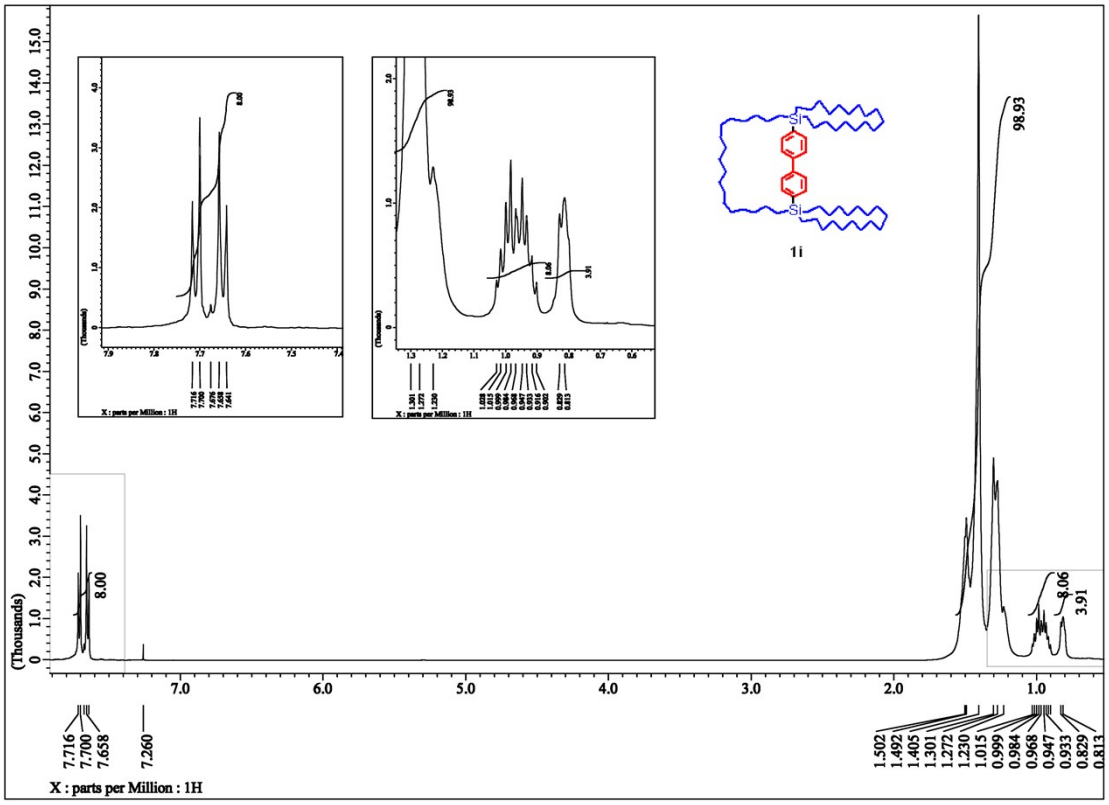


**Fig S7.** $^{1}$H NMR spectrum of Biphenylene-bridged Molecular Gyrotop Isomer (**1i**) in $CDCl_3$.

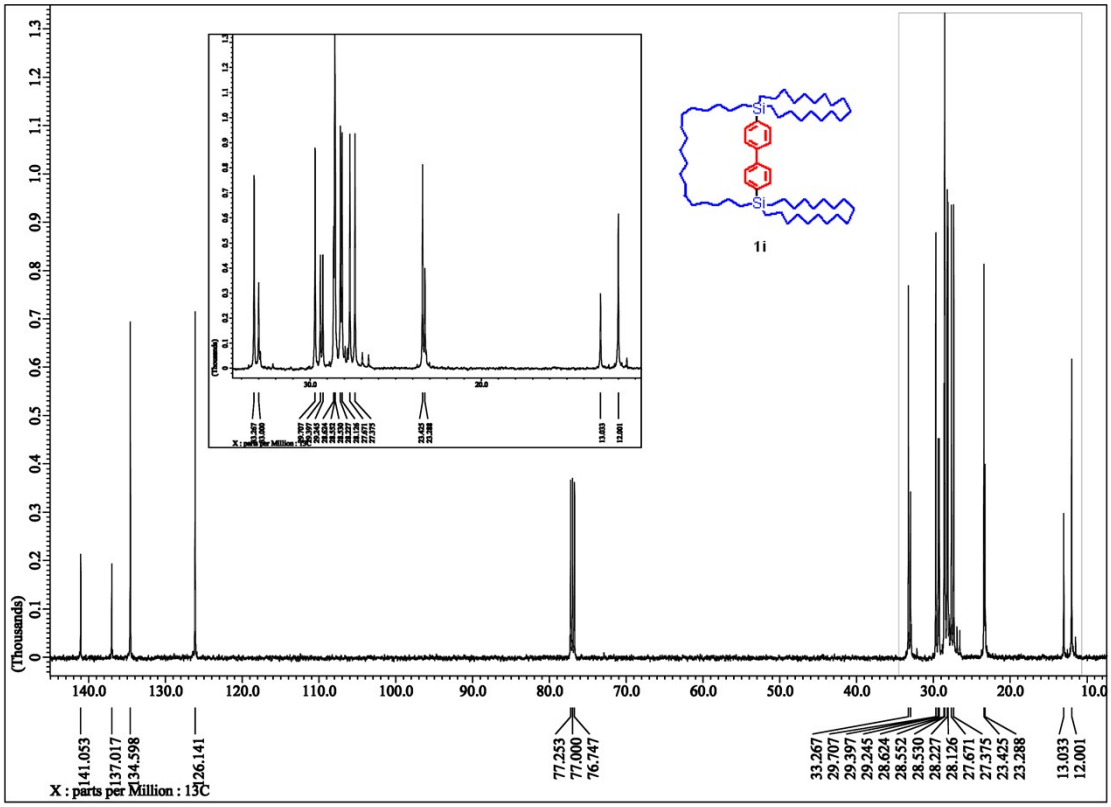


**Fig S8.** $^{13}$C{$^{1}$H} NMR spectrum of Biphenylene-bridged Molecular Gyrotop Isomer (**1i**) in $CDCl_3$.

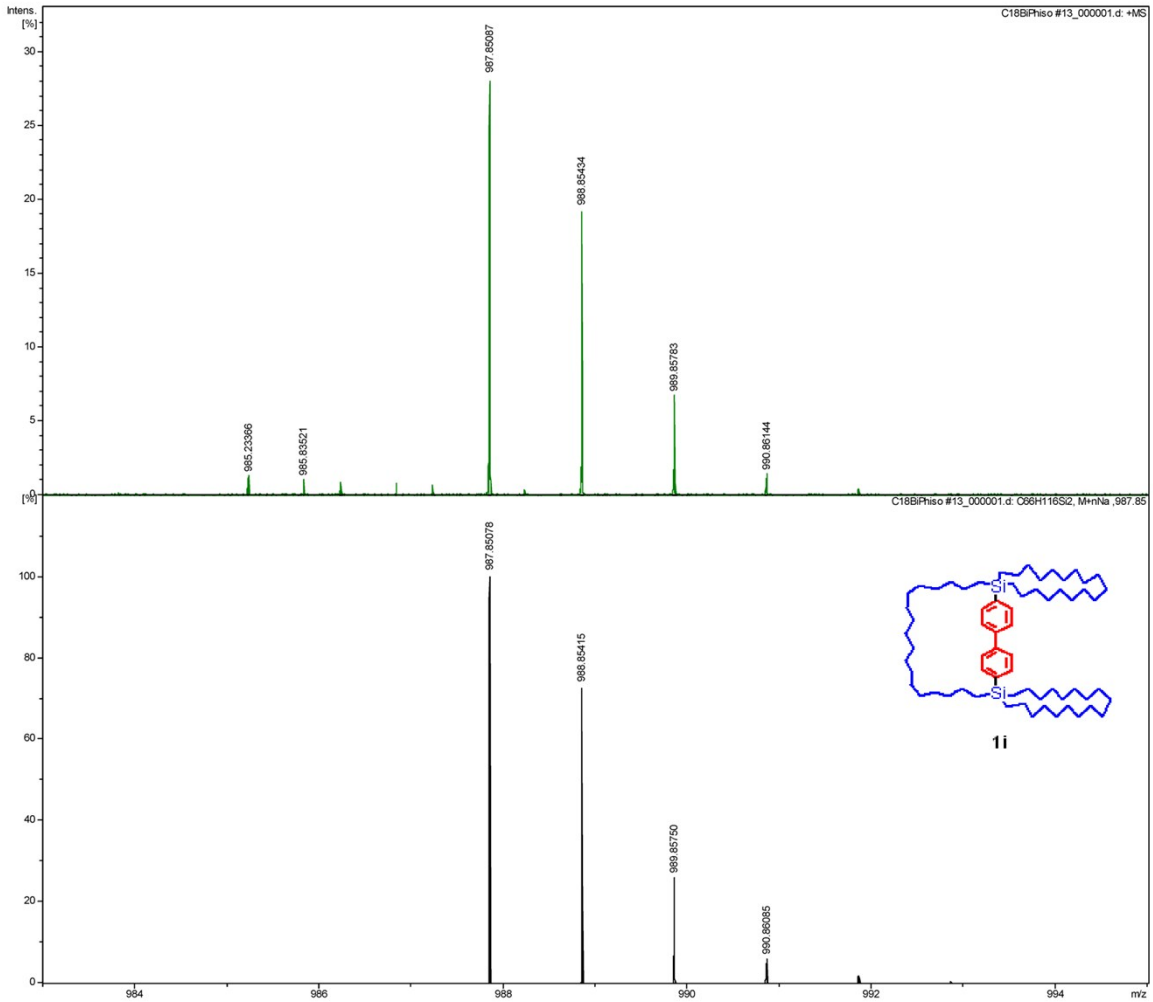


**Fig S9.** HRMS spectrum of Biphenylene-bridged Molecular Gyrotop Isomer (**1i**) (ESI, positive). Top: obsd. Bottom: sim.

**d. Spectra of 4,4'-Bis(tri-9-decenylsilyl)biphenyl (2-$d_4$)**

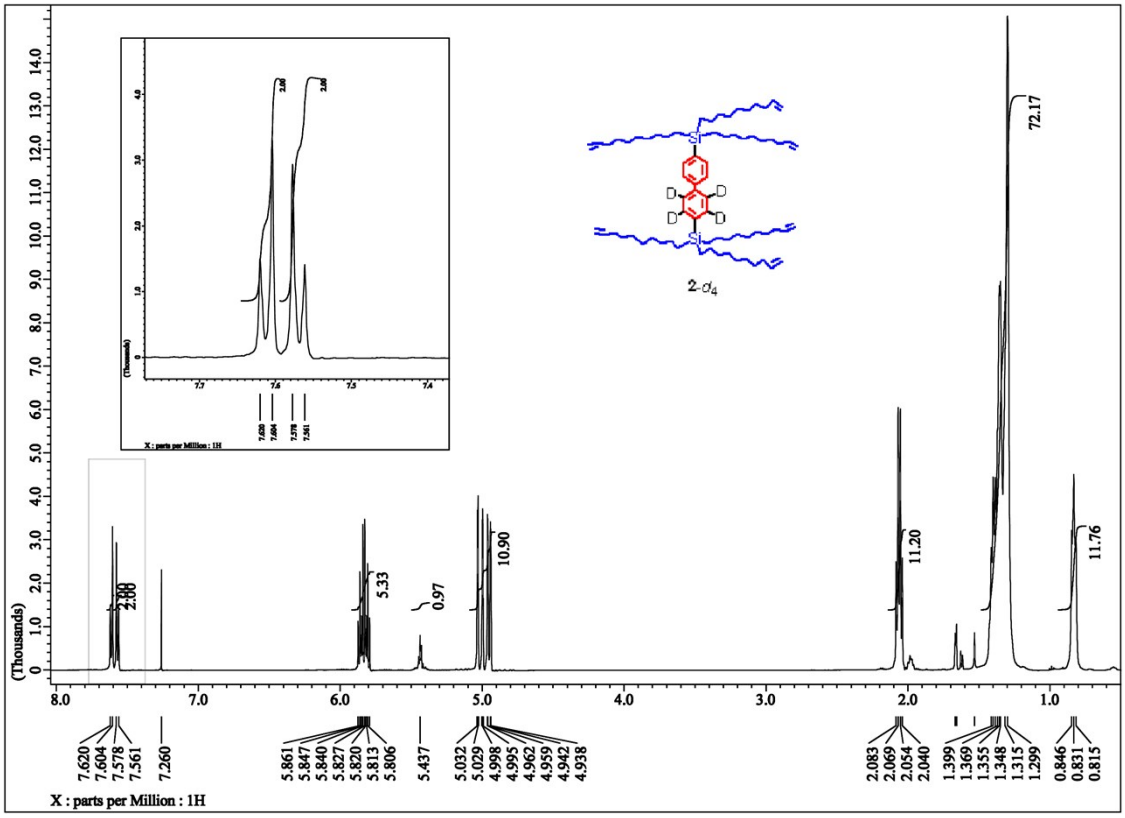


**Fig S10.** $^{1}$H NMR spectrum of Deuterated 4,4'-Bis(tri-9-decenylsilyl)biphenyl (**2-$d_4$**) in $CDCl_3$.

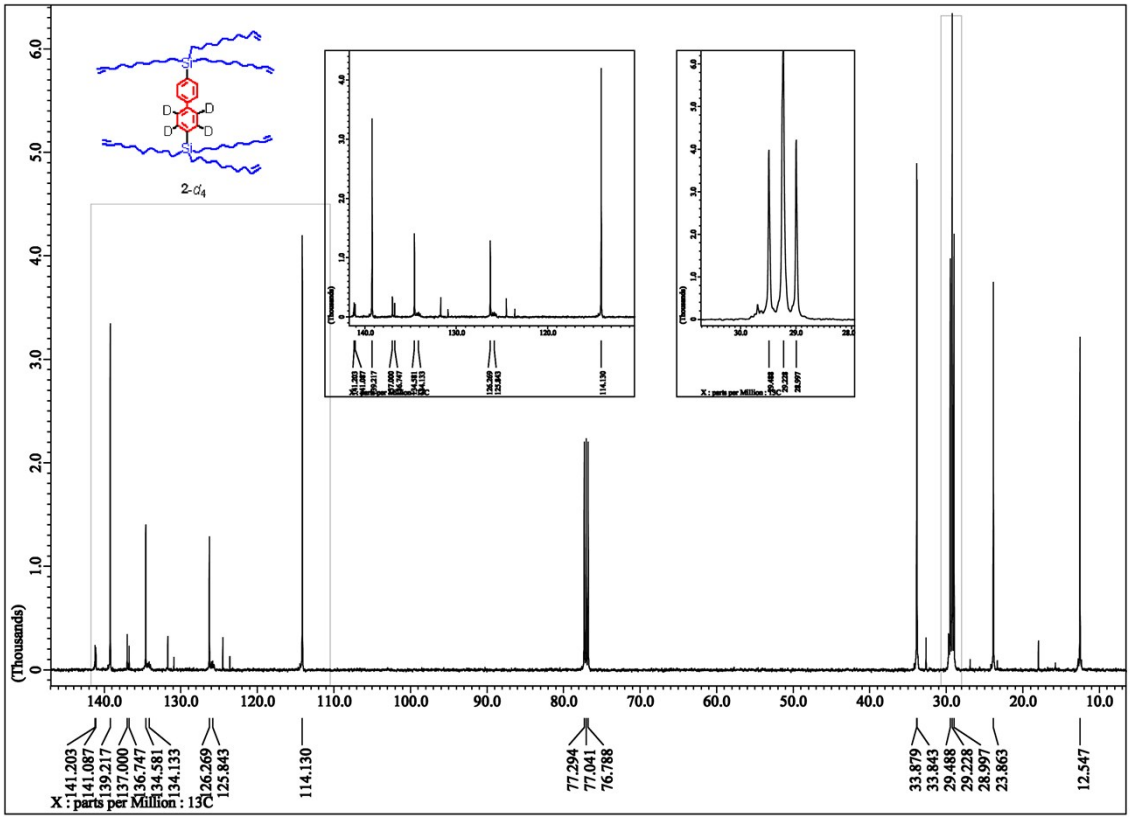


**Fig S11.** $^{13}$C{$^{1}$H} NMR spectrum of Deuterated 4,4'-Bis(tri-9-decenylsilyl)biphenyl (**2-$d_4$**) in $CDCl_3$.

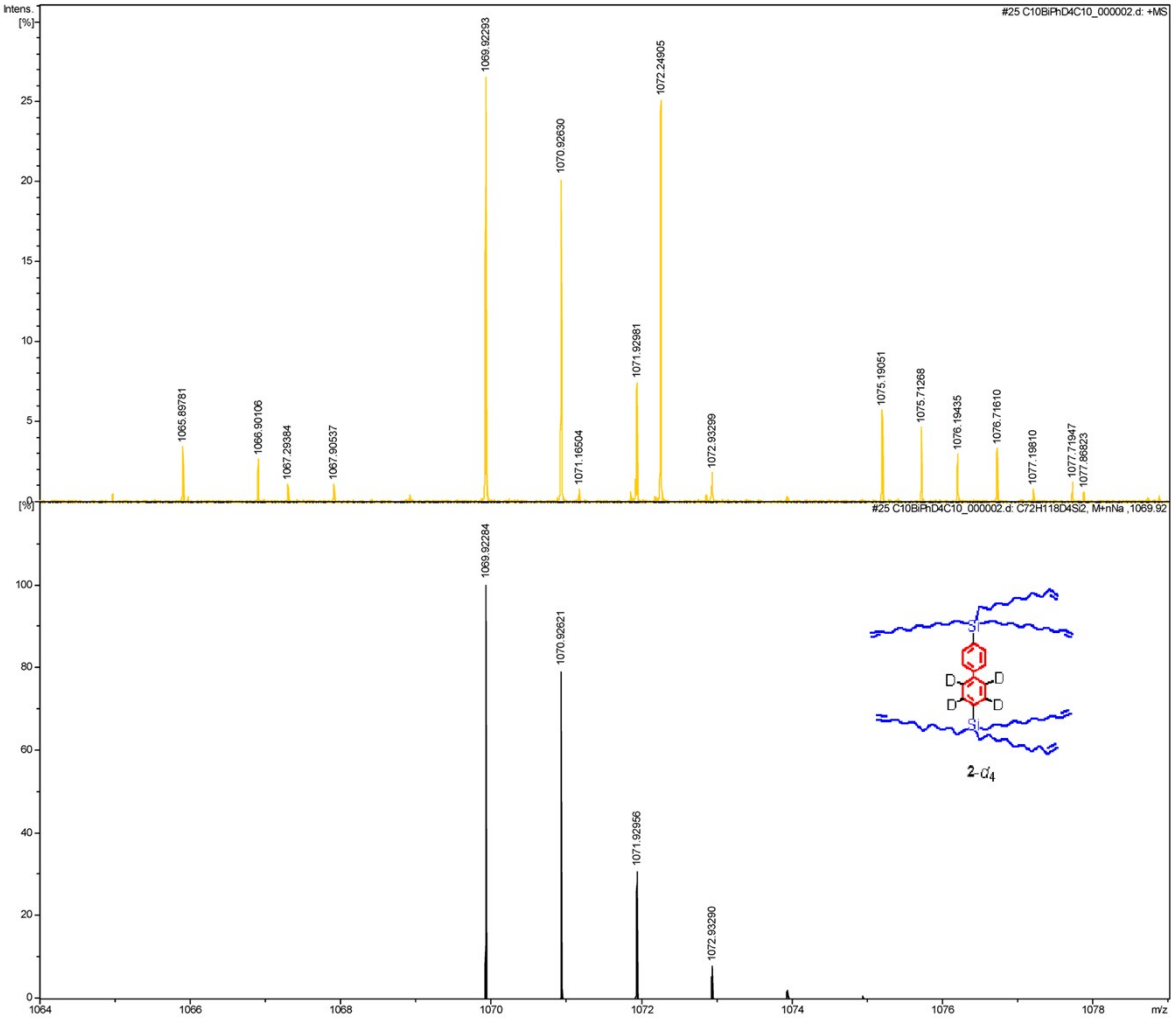


**Fig S12.** HRMS spectrum of Deuterated 4,4'-Bis(tri-9-decenylsilyl)biphenyl (**2-*d*$_4$**) (ESI, positive). Top: obsd. Bottom: sim.

**e. Spectra of Deuterated Biphenylene-bridged Molecular Gyrotop (1-$d_4$)**

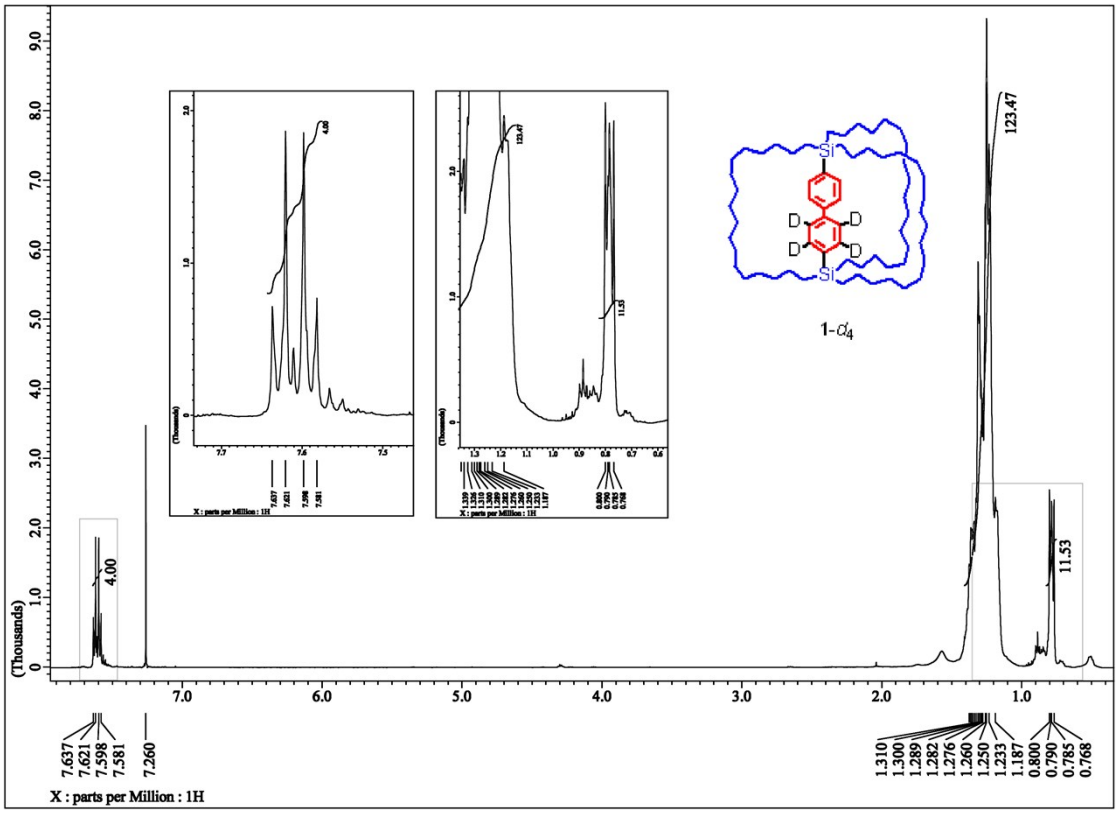


**Fig S13.** $^1$H NMR spectrum of Deuterated Biphenylene-bridged Molecular Gyrotop (**1-$d_4$**) in $CDCl_3$.

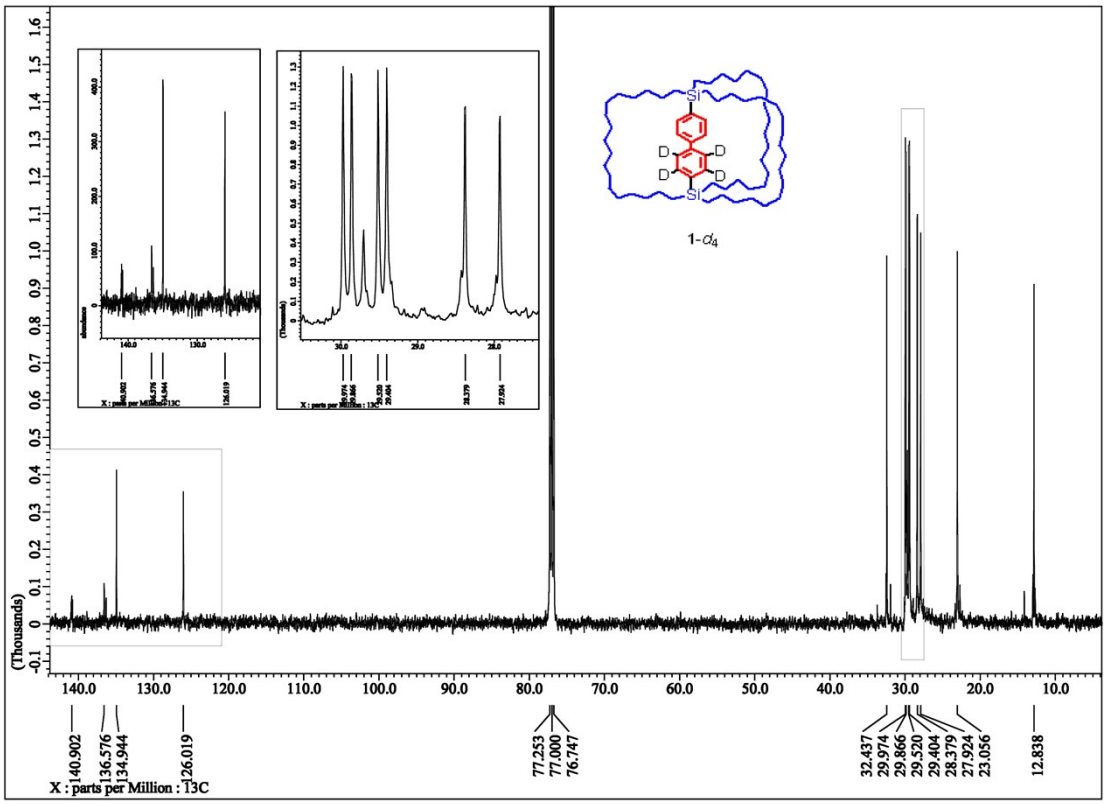


**Fig S14.** $^{13}$C{$^1$H} NMR spectrum of Deuterated Biphenylene-bridged Molecular Gyrotop (**1-$d_4$**) in $CDCl_3$.

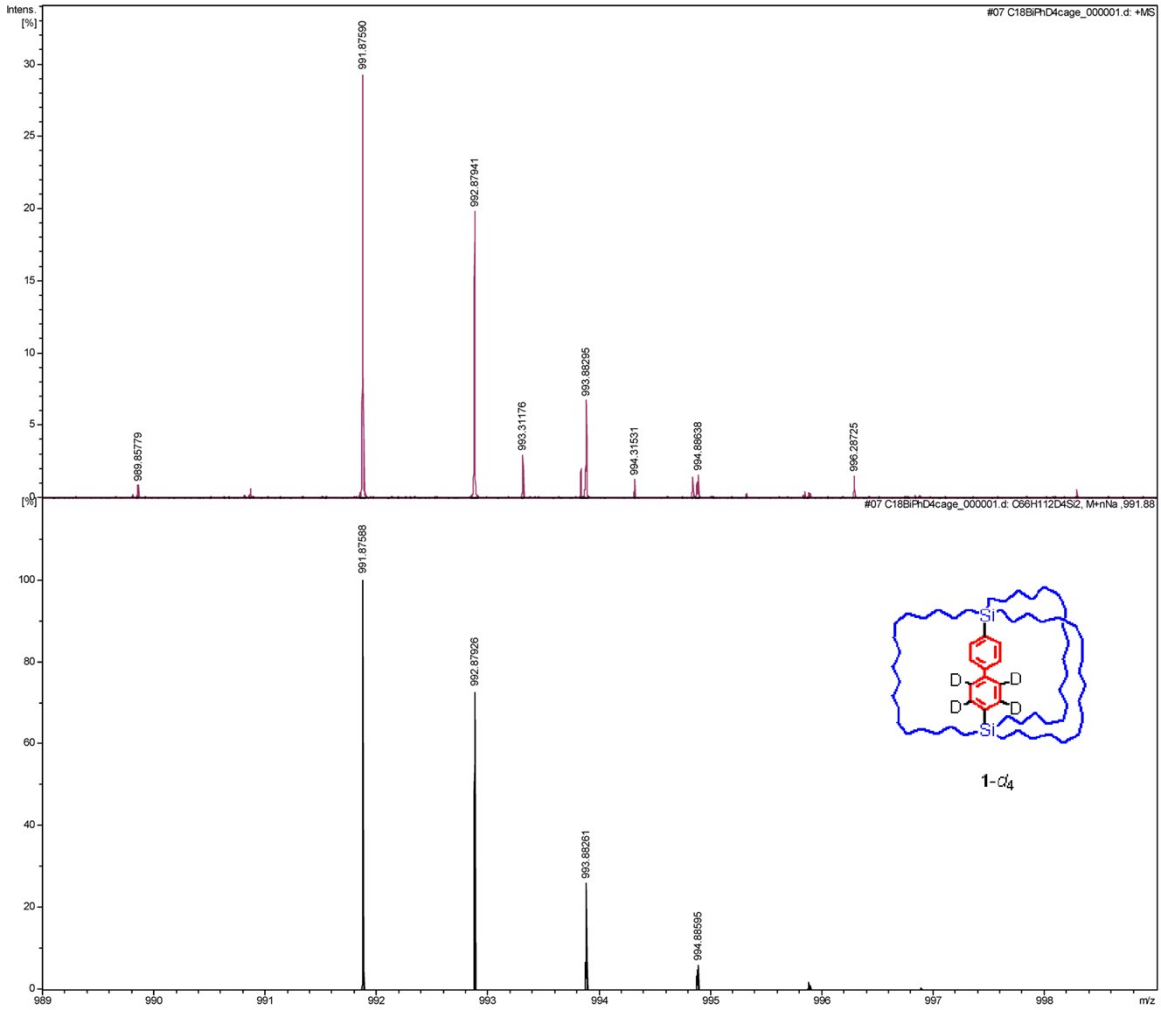


**Fig S15.** HRMS spectrum of Deuterated Biphenylene-bridged Molecular Gyrotop (**1-*d*$_4$**) (ESI, positive). Top: obsd. Bottom: sim.

## 2. Details of X-ray Crystallography of Moleculr Gyrotop 1

The structures were refined using a SHELXL program package. Because of remarkably weak diffraction data at high temperature at 280 K and 320 K, it was difficult to refine the structure of the crystal adequately. Certain C-C distances and C-C-C angles of the alkyl chains were restrained by means of DFIX and DANG, respectively, because of the unresolved disorder.

**Table S1.** Crystal Data of **2** at 260 K, 300 K, and 340 K

| | | **200 K** | **280 K** | **320 K** |
|---|---|---|---|---|
| **CCDC #** | | 1554865 | 1554866 | 1554867 |
| **Empirical formula** | | $C_{66}H_{116}Si_2$ | $C_{66}H_{116}Si_2$ | $C_{66}H_{116}Si_2$ |
| **Cryst shape** | | prism | plate | prism |
| **Cryst color** | | colorless | colorless | colorless |
| **Cryst size** | | 0.400 x 0.400 x 0.050 $mm^3$ | 0.400 x 0.400 x 0.300 $mm^3$ | 0.400 x 0.400 x 0.300 $mm^3$ |
| **Formula weight / g $mol^{-1}$** | | 965.77 | 965.77 | 965.77 |
| **Crystal system** | | Monoclinic | Monoclinic | Monoclinic |
| **Space group** | | C2/c | Cc | Cc |
| **Z** | | 4 | 4 | 4 |
| **Temperature / K** | | 200(2) | 280(2) | 320(2) |
| **Cell parameter** | *a* | 35.097(3) Å | 36.52(3) Å | 36.88(3) Å |
| | *b* | 11.4728(10) Å | 10.968(9) Å | 11.065(8) Å |
| | *c* | 16.9361(14) Å | 19.057(16) Å | 19.195(13) Å |
| | $\alpha$ | 90.00° | 90.00° | 90.00° |
| | $\beta$ | 110.809(1)° | 120.161(12)° | 121.141(8)° |
| | $\gamma$ | 90.00° | 90.00° | 90.00° |
| | *V* | 6374.6(9) $Å^3$ | 6600(10) $Å^3$ | 6703(8) $Å^3$ |
| **Calculated density** | | 1.006 $Mg/m^3$ | 0.972 $Mg/m^3$ | 0.957 $Mg/m^3$ |
| **F(000)** | | 2160 | 2160 | 2160 |
| **Absorption coefficient** | | 0.091 $mm^{-1}$ | 0.088 $mm^{-1}$ | 0.087 $mm^{-1}$ |
| **$\theta$ range for collecn (deg)** | | 1.241 to 27.932° | 1.290 to 27.775° | 1.950 to 27.980° |
| **Index ranges** | | -40<=h<=46, -15<=k<=6, -21<=l<=22 | -47<=h<=46, -12<=k<=13, -23<=l<=24 | -48<=h<=18, -13<=k<=14, -23<=l<=25 |
| **Reflections collected** | | 17101 | 17562 | 18001 |
| **Independent reflections** | | 7008 [R(int) = 0.0242] | 11397 [R(int) = 0.0377] | 9394 [R(int) = 0.0545] |
| **Completeness** | | 99.9 % | 99.8 % | 99.8 % |
| **Goodness-of-fit on $F^2$** | | 1.063 | 0.955 | 0.954 |
| **Final R indices [I>2sigma(I)]** | | R1 = 0.0837, wR2 = 0.2458 | R1 = 0.1208, wR2 = 0.3104 | R1 = 0.1291, wR2 = 0.3138 |
| **R indices (all data)** | | R1 = 0.1177, wR2 = 0.2783 | R1 = 0.3565, wR2 = 0.4710 | R1 = 0.3692, wR2 = 0.4925 |
| **Largest diff. peak and hole** | | 0.558 and -0.629 e.$Å^{-3}$ | 0.253 and -0.126 e.$Å^{-3}$ | 0.305 and -0.148 e.$Å^{-3}$ |

## 3. Details of Solid-State $^2$H NMR Study of 1-$d_4$

### a. Temperature Dependent Solid state $^2$H NMR spectra of 1-$d_4$.

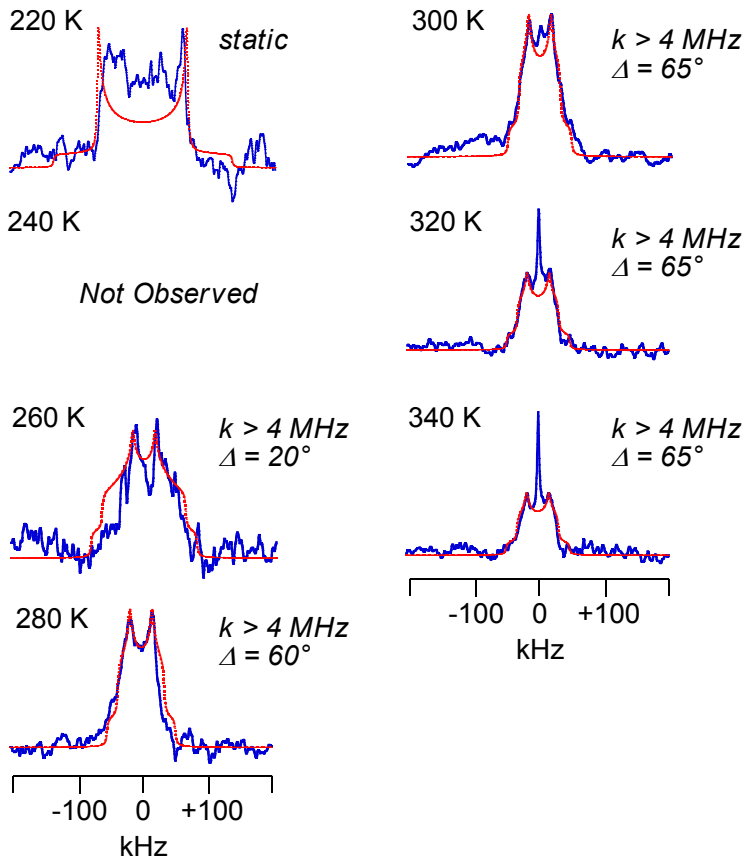


**Fig S16.** Temperature dependence of solid-state $^2$H NMR spectra of **1**-$d_4$ [solid black line: observed spectra; dotted red line: spectra simulated by assuming 180º flipping with designated exchange rate constants, $k$, and degree of angular displacement, $\Delta$.].

## 4. Details of Optical Properties of a Single Crystal of 1

The fast and slow optical axes were confirmed by a polarized-light microscope equipped with a sensitive color plate. Retardations were observed by the polarized-light microscope equipped with a Berek compensator and monochromatic light at 546 nm generated by a color filter. The thickness of the crystal was measured by a laser displacement sensor at 300 K. The $\Delta n$ value was calculated from the retardation/thickness of the sample.

### a. Crystal orientation mapping of a single crystal of 1

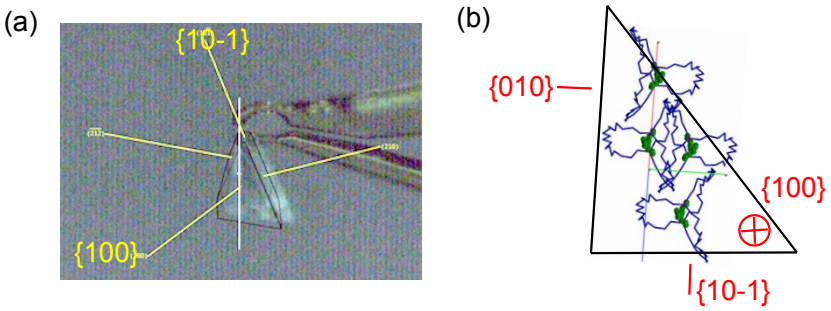


**Fig S17.** Crystal orientation mapping of a single crystal of **2** as determined by X-ray diffraction study at 300 K; (a) observed data, (b) schematic drawing.

### b. Thickness of the single crystal of 1

The thickness of the crystal was measured at 300 K using a laser displacement sensor.

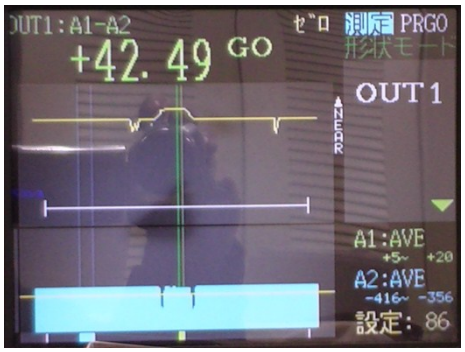


**Fig S18.** Measurement of the thickness of the single crystal of **2** at 300 K using a laser displacement sensor; The thickness is 42.5 ± 1 μm.

## c. Photograph of single crystals of 1 observed by polarized microscopy

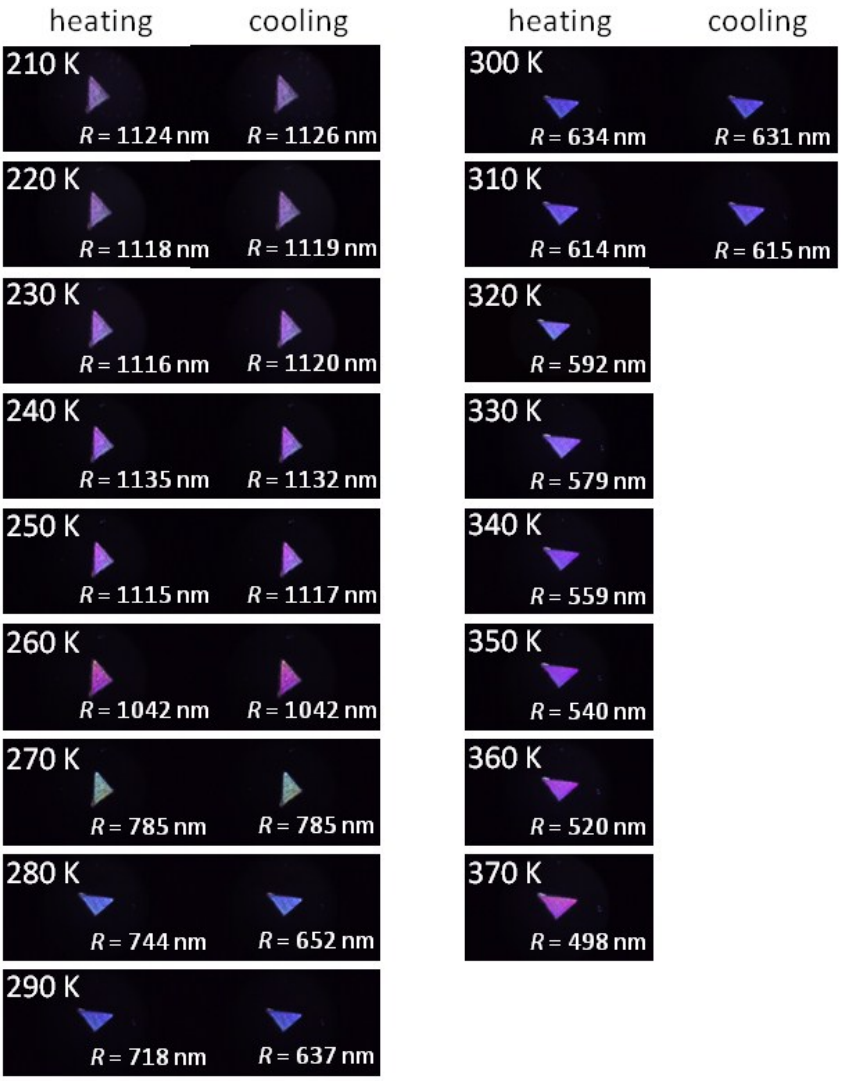


**Fig S19.** Photographs of the single crystal of **1** (sample thickness: 42.5 ± 1 μm) showing the crystal face upon irradiation with polarized white light ({100} face).

## d. Temperature dependence of Δ*n* of 1

Temperature dependence of birefringence (Δ*n*) of the crystal face of a single crystal of **1**, calculated from Retardation/Thickness as summarized in Table S2.

**Table S2.** Temperature Dependence of Retardation, and Δ*n* of **1** (Sample Thickness $d$ = 42.5 ± 1 μm)

| Temperature / K | Retardation [1] / nm | | Δ*n* [2] / $10^{-3}$ | |
|---|---|---|---|---|
| | heating process | cooling process | heating process | cooling process |
| 210 | 1124.4 ± 8.6 | 1125.5 ± 3.9 | 2.647 ± 0.082 | 2.650 ± 0.072 |
| 220 | 1117.5 ± 2.4 | 1119.0 ± 3.9 | 2.631 ± 0.068 | 2.635 ± 0.071 |
| 230 | 1115.9 ± 6.8 | 1120.3 ± 2.9 | 2.627 ± 0.078 | 2.638 ± 0.069 |
| 240 | 1135.2 ± 7.1 | 1132.0 ± 0.7 | 2.673 ± 0.080 | 2.665 ± 0.064 |
| 250 | 1115.4 ± 2.7 | 1116.7 ± 4.6 | 2.626 ± 0.068 | 2.629 ± 0.073 |
| 260 | 1041.6 ± 5.2 | 1042.4 ± 5.9 | 2.452 ± 0.070 | 2.454 ± 0.072 |
| 270 | 785.1 ± 3.1 | 784.8 ± 3.7 | 1.849 ± 0.051 | 1.848 ± 0.052 |
| 280 | 744.2 ± 1.4 | 651.5 ± 3.0 | 1.752 ± 0.045 | 1.534 ± 0.043 |
| 290 | 718.0 ± 4.9 | 637.0 ± 3.3 | 1.691 ± 0.051 | 1.500 ± 0.043 |
| 300 | 634.4 ± 3.3 | 631.7 ± 2.8 | 1.494 ± 0.043 | 1.487 ± 0.042 |
| 310 | 613.5 ± 4.2 | 614.8 ± 6.0 | 1.444 ± 0.036 | 1.448 ± 0.048 |
| 320 | 592.4 ± 2.7 | | 1.395 ± 0.039 | |
| 330 | 578.6 ± 3.2 | | 1.362 ± 0.040 | |
| 340 | 559.1 ± 3.0 | | 1.316 ± 0.038 | |
| 350 | 540.2 ± 1.2 | | 1.272 ± 0.033 | |
| 360 | 520.5 ± 2.2 | | 1.226 ± 0.034 | |
| 370 | 498.3 ± 0.8 | | 1.173 ± 0.030 | |

1) Mean values of three time measurements.
2) The error for the birefringence Δ*n* includes both a measurement error of retardation and a thickness error (± 1.0).

## e. Details of measurement of the optical axes of the single crystal of 1

On the {100}-face of the crystal at 300 K, the fast optical axis is observed to be parallel to <010> axis as ascertained from the decrease in the retardation by 147 nm, observed using a polarized-light microscope equipped with a 1/4λ plate, which adds 147 nm along the <010> axis (Fig S20iib). After rotation of the crystal by 90°, the retardation observed through the 1/4λ plate increased by 147 nm (Fig S20iic), indicating that the slow optical axis is perpendicular to <010> axis. On the other hand, in the case at 260 K the increment and decrement of the retardation observed through the 1/4λ plate were opposite to that observed at 300 K (Fig S20i).

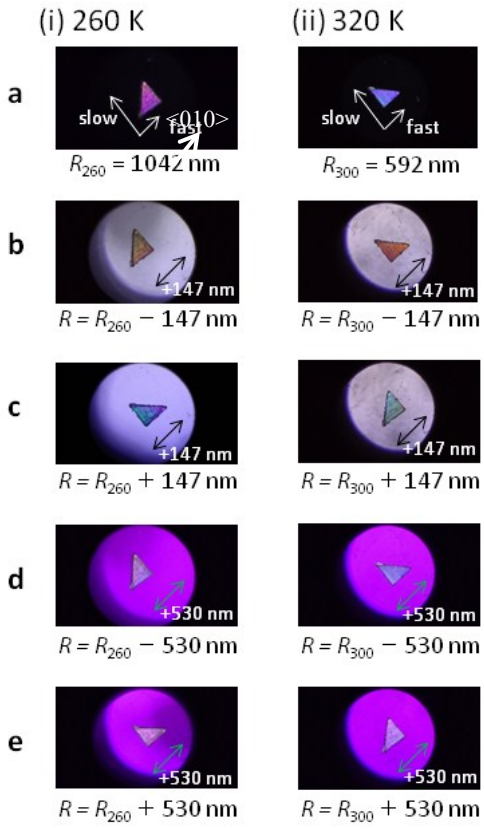


**Fig S20.** Photographs of the single crystals of **1** (sample thickness: 42.5 ± 1.0 μm) on the crystal face upon irradiation with polarized white light and its retardation ($R$) ({100} face). **a**, Normal photograph with directions of optical axes. **b**, Photograph through a 1/4λ plate. **c**, Photograph through a 1/4λ plate after 90° rotation of the crystal. **d**, Photograph through a sensitive color plate. **e**, Photograph through a sensitive color plate after 90° rotation of the crystal.